IJMMM International Journal of Minerals, Metallurgy and Materials 矿物冶金与材料学报（英文版）

Isothermal kinetic analysis on reduction of solid/liquid wustite by hydrogen

Jianliang Zhang, Yang Li, Zhengjian Liu, Tengfei Wang, Yaozu Wang, Kejiang Li, Guilin Wang, Tao Xu, and Yong Zhang

Cite this article as:
Jianliang Zhang, Yang Li, Zhengjian Liu, Tengfei Wang, Yaozu Wang, Kejiang Li, Guilin Wang, Tao Xu, and Yong Zhang, Isothermal kinetic analysis on reduction of solid/liquid wustite by hydrogen, *Int. J. Miner. Metall. Mater.*, 29(2022), No. 10, pp. 1830-1838. https://doi.org/10.1007/s12613-022-2518-0

Articles you may be interested in

Jue Tang, Man-sheng Chu, Feng Li, Cong Feng, Zheng-gen Liu, and Yu-sheng Zhou, Development and progress on hydrogen metallurgy, *Int. J. Miner. Metall. Mater.*, 27(2020), No. 6, pp. 713-723. https://doi.org/10.1007/s12613-020-2021-4

Feng Li, Qing-jie Zhao, Man-sheng Chu, Jue Tang, Zheng-gen Liu, Jia-xin Wang, and Sheng-kang Li, Preparing high-purity iron by direct reductionsmelting separation of ultra-high-grade iron concentrate, *Int. J. Miner. Metall. Mater.*, 27(2020), No. 4, pp. 454-462. https://doi.org/10.1007/s12613-019-1959-6

Yuan Li, Li-na Cheng, Wen-kang Miao, Chun-xiao Wang, De-zhi Kuang, and Shu-min Han, Nd–Mg–Ni alloy electrodes modified by reduced graphene oxide with improved electrochemical kinetics, *Int. J. Miner. Metall. Mater.*, 27(2020), No. 3, pp. 391-400. https://doi.org/10.1007/s12613-019-1880-z

Ying-yi Zhang, Wei Lü, Xue-wei Lü, Sheng-ping Li, Chen-guang Bai, Bing Song, and Ke-xi Han, Isothermal reduction kinetics of Panzhihua ilmenite concentrate under 30vol% CO-70vol% N_2 atmosphere, *Int. J. Miner. Metall. Mater.*, 24(2017), No. 3, pp. 240-248. https://doi.org/10.1007/s12613-017-1401-x

Bo Wang, Chao-yi Chen, Jun-qi Li, Lin-zhu Wang, Yuan-pei Lan, and Shi-yu Wang, Solid oxide membrane-assisted electrolytic reduction of Cr_2O_3 in molten $CaCl_2$, *Int. J. Miner. Metall. Mater.*, 27(2020), No. 12, pp. 1626-1634. https://doi.org/10.1007/s12613-020-2141-x

Shi-chao Wu, Zheng-yao Li, Ti-chang Sun, Jue Kou, and Xiao-hui Li, Effect of additives on iron recovery and dephosphorization by reduction roasting–magnetic separation of refractory high-phosphorus iron ore, *Int. J. Miner. Metall. Mater.*, 28(2021), No. 12, pp. 1908-1916. https://doi.org/10.1007/s12613-021-2329-8

IJMMM WeChat

QQ author group

International Journal of Minerals, Metallurgy and Materials
Volume 29, Number 10, October 2022, Page 1830
https://doi.org/10.1007/s12613-022-2518-0

Isothermal kinetic analysis on reduction of solid/liquid wustite by hydrogen

Jianliang Zhang[1,2], *Yang Li*[1], *Zhengjian Liu*[1]✉, *Tengfei Wang*[1], *Yaozu Wang*[3]✉, *Kejiang Li*[1], *Guilin Wang*[1], *Tao Xu*[4], *and Yong Zhang*[4]

1) School of Metallurgical and Ecological Engineering, University of Science and Technology Beijing, Beijing 100083, China
2) School of Chemical Engineering, The University of Queensland, St Lucia, QLD 4072, Australia
3) Institute of Artificial Intelligence, University of Science and Technology Beijing, Beijing 100083, China
4) Inner Mongolia CISP Technology Co., Ltd., Wuhai 016000, China
(Received: 8 March 2022; revised: 31 May 2022; accepted: 6 June 2022)

Abstract: Isothermal thermogravimetric analysis was used to study the reduction process of solid/liquid wustite by hydrogen. Results show that wustite in both states can be reduced entirely at all temperatures. The thermal and kinetic conditions for the hydrogen reduction of molten phases are better than those when the reactants and products are in the solid state, with a higher reaction rate. The hydrogen reduction of different wustite phases fits the Mampel Power model (power exponent $n = 1/2$) well, and this model is independent of the phase state. The average apparent activation energies of the reduction process calculated by the iso-conversional method are 5.85 kJ·mol^{-1} and 104.74 kJ·mol^{-1}, when both reactants and products are in the solid state and the molten state, respectively. These values generally agree with those calculated by the model fitting method.

Keywords: hydrogen metallurgy; iron oxide; smelting reduction; reduction kinetics

1. Introduction

Under the condition of carbon neutrality for the whole world, carbon emission reduction has become the primary path for the new trend of green and clean development of the iron and steel industry [1–3]. The application of hydrogen technology provides a new idea for the steel industry to achieve the goals of carbon peaking and carbon neutralization especially in China. Hydrogen metallurgy has become the clean, efficient, and pollution-free steelmaking technology direction of exploration in different countries [4–8]. Scholars worldwide have extensively researched the hydrogen reduction of iron oxides, and solid iron oxides are the primary reduction object, namely the "gas–solid" reaction process [9–14]. With the continuous development of smelting reduction technology, the application of hydrogen in the smelting reduction ironmaking process provides a new possibility for further carbon emission reduction [15–17].

The reduction of molten iron oxides by hydrogen has been studied from different perspectives. Katayama *et al.* [18] conducted the hydrogen reduction of FeO in molten slag at simulated blast furnace conditions at the temperature of 1450°C, using an MgO crucible as the reaction vessel. The results showed that the diffusion rate of FeO in the slag was 3×10^{-4} cm^2·s^{-1}. However, whether the material of the MgO crucible affects the reduction process was not explained. Ban-Ya *et al.* [19] studied the hydrogen reduction of molten FeO by using a thermal analytical balance at 1400 and 1450°C, and an iron crucible was used as the reaction vessel to ensure that the initial melting reduction was pure FeO. The experimental results show that when the chemical reaction determined the reduction reaction rate, the estimated apparent chemical reaction rate constant was 1.6×10^{-7} g of oxygen/(cm^2·s·Pa), about 20 times the reaction rate of solid FeO reduction by hydrogen. Hayashi and Iguchi [20] studied the effect of hydrogen on the reduction of molten wustite particles using a thin particle gas-phase transport reaction system, at the temperature range of 1450–1550°C and a hydrogen ratio of 5vol%–30vol%. The results indicated that chemical reaction was the limiting factor of the reduction, and the activation energy was calculated to be 110 kJ·mol^{-1}. Nagasaka *et al.* [21] and Seftejani and Schenk [22] summarized the reduction rates of molten pure FeO by solid carbon, dissolved carbon, CO, and H_2. They found that the reaction rate of reduction by hydrogen was one or two orders of magnitude higher than that of other reducing agents.

However, the research on hydrogen reduction of molten iron oxides is insufficient compared with the hydrogen reduction of solid iron oxides. Moreover, most previous studies were conducted at the temperature range where the reactant FeO was molten while the product (iron) was in a solid state. Therefore, in this paper, thermogravimetric analyses were carried out on the reduction of pure solid wustite (ferrous metal is in solid state) and pure molten wustite (ferrous

✉ Corresponding authors: Zhengjian Liu E-mail: liuzhengjian@ustb.edu.cn; Yaozu Wang E-mail: wgyozu@163.com

metal is in molten state) by hydrogen. The differences between the reaction processes of hydrogen reduction of solid FeO samples and liquid FeO samples were compared in this paper. The kinetics parameters of hydrogen reduction of different wustite phases were analyzed and compared using iso-conversional method and model fitting method.

2. Experimental

2.1. Materials

The FeO reagent used in this paper was prepared with reduced iron powder and Fe_3O_4 reagent (analytical grade) [19,23–24]. The reduced iron powder and Fe_3O_4 reagent were mixed homogeneously according to the mole ratio of 1.5:1 ($Fe : Fe_3O_4$), to ensure the iron oxide in the test was pure FeO. Then the mixture was put into a well-sealed tubular furnace. The temperature of furnace was firstly raised to 850°C and kept constant for 2 h, then decreased to ambient temperature. Argon was injected into the furnace at a flow rate of 3 $L \cdot min^{-1}$ throughout the process. Studies [25] have shown that the FeO sample powder prepared in the laboratory can be stably stored at normal temperature for at least 90 d. The prepared FeO powder was placed in an airtight container and sealed with nitrogen to improve the accuracy of the experiment. X-ray diffraction (XRD; Bruker D8 Advance, 40 kV/40 mA, Cu-K_α) analysis for prepared FeO powder was shown in Fig. 1(a), only FeO characteristic peaks exist in the XRD spectrum. The chemical analysis results showed that FeO content in the product was 90.37wt%, and the rest was metallic iron. The particle size of the FeO sample was analyzed via laser particle test (Malven Instruments), and the results shown in Fig. 1(b) indicated that the size of the FeO sample was smaller than 74 μm.

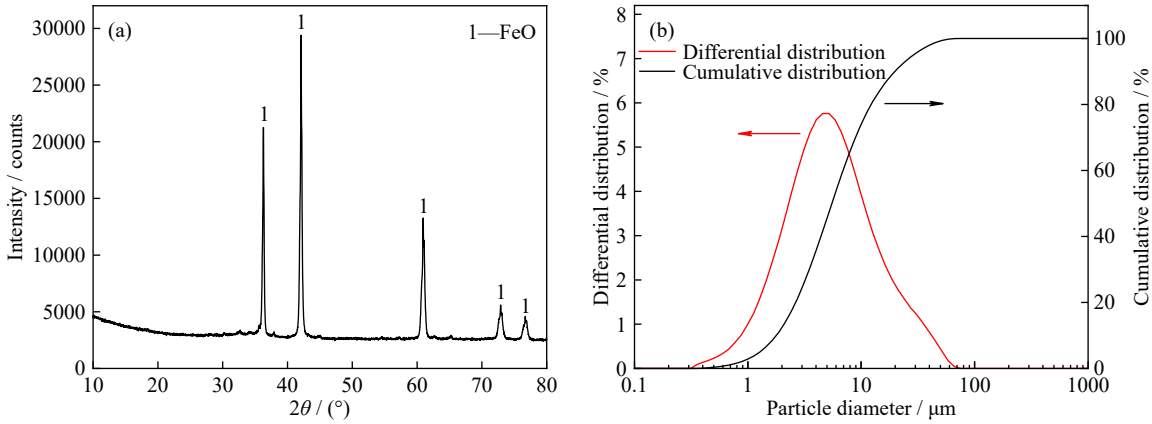

Fig. 1. (a) X-ray diffraction and (b) particle size distribution results of FeO sample.

2.2. Experimental methods

Setaram Ultra-high temperature thermal analyzer (Setsys EVO TG-DTA 1750) was used for FeO reduction tests at different temperatures, and Fig. 2 shows the schematic diagram of the equipment. The maximum range of the device is 100 g with a weighing accuracy of 0.3 μg, and the maximum temperature can reach 1750°C. 20 mg FeO sample prepared was first packed inside a platinum crucible at room temperature, and then placed in the thermogravimetry (TG) analyzer and heated to experimental temperature at a heating rate of 30°C·min^{-1} under N_2 atmosphere (>99.999%). The temperature was then held for 30 min under N_2 atmosphere to ensure the sample temperature was stable, after which, the gas was converted to the reducing gas. A blank test was carried out in a crucible without samples under the same test conditions to exclude the effects of systematic errors in the thermal analyzer and the buoyancy of the reaction gas. The weight loss data were obtained from the isothermal reduction stage, and the thermal analysis data from the blank test were deducted.

In order to compare the difference of wustite reduction by hydrogen in different phase states, experiment temperatures were designed in all molten for both wustite and metal iron according to the melting point of wustite (1369°C) and metal iron (1538°C). For comparison, all solid for wustite and metal iron were also used as reductive reactants. The specific experimental conditions are shown in Table 1.

The reduction conversion (α) is calculated by Eq. (1):

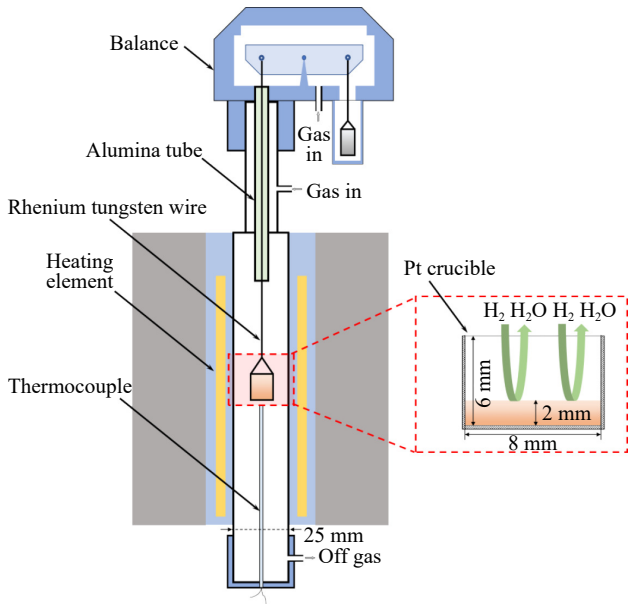

Fig. 2. Schematic diagram of TG analyzer.

Table 1. Experimental conditions on isothermal reduction of wustite

Temperature / °C	Phase morphology	Gas flow / (mL·min^{-1})	Gas composition
900	FeO: solid; Fe: solid	20	100% H_2
1100			
1300			
1540	FeO: melting; Fe: melting		
1560			
1580			

$$\alpha = \frac{m_0 - m_t}{m_0 - m_\infty} \quad (1)$$

where α is the reduction conversion of the sample at a specific time t; m_0 is the initial mass of the sample, g; m_t is the mass of the sample at a particular time t, g; m_∞ is the mass of the sample at the end of the experiment, g.

3. Results and discussion

3.1. Repeatability of the experiment results

The stability of the experiment is crucial to the accurate analysis of the experimental results. Therefore, two tests with the same conditions were designed at 1300 and 1560°C to verify the stability of the equipment and the repeatability of the test, and the results are shown in Fig. 3. The two reduction conversion curves at the same experimental conditions are highly overlapped, indicating that the tests have good repeatability and reliable results.

3.2. Reduction conversion and rate

The reduction conversion curves at different gas flow rates were investigated by pre-experiments to evaluate and eliminate the effect of external diffusion on the reduction. When the temperature reached 1560°C, the reducing gas with gas flow rates of 10, 15, 20, and 25 mL/min was blown into the system. Fig. 4 shows the reduction conversion and conversion rate curves of samples reduced at different reducing gas flow rates. The reduction conversion (α) and conversion rate ($d\alpha/dt$) curves at reducing gas flow rate of 20 mL/min are almost the same as those at 25 mL/min, with a difference of only about 4%. Therefore, the reducing gas flow rate was selected as 20 mL/min in the subsequent reduction experiments.

Fig. 5 shows the reduction conversion curves for the reduction of solid/molten wustite by hydrogen at different temperatures. The complete reduction can be achieved regardless of the reduction temperature and phase states, i.e., the reduction conversion could reach 1.0. When the reduction time is 600 s, the reduction conversion increases from 0.2070 to 0.3205 with the temperature increasing from 900 to 1300°C for solid wustite and metal iron. Moreover, it increases from 0.5673 to 0.8589 when the temperature increases from 1540 to 1580°C for molten wustite and metal iron. It means that

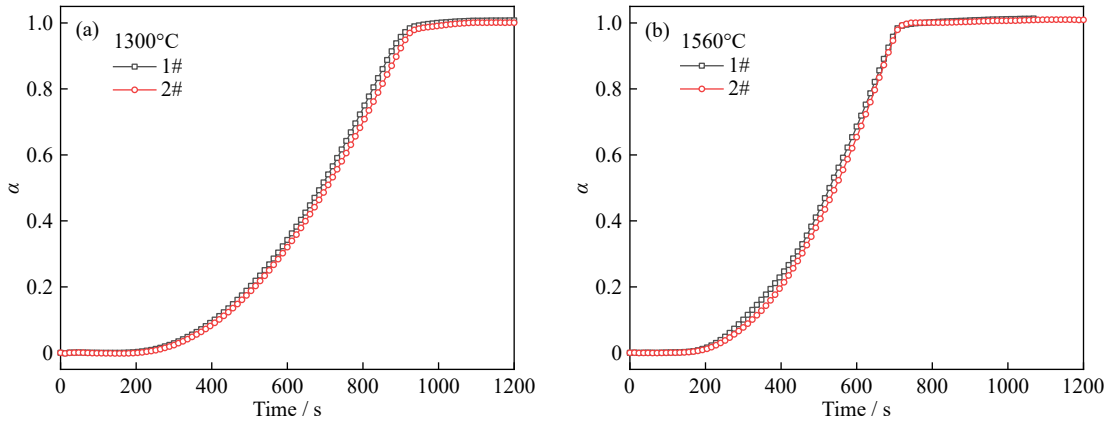

Fig. 3. Repeatability of the experiment results: (a) 1300°C; (b) 1560°C.

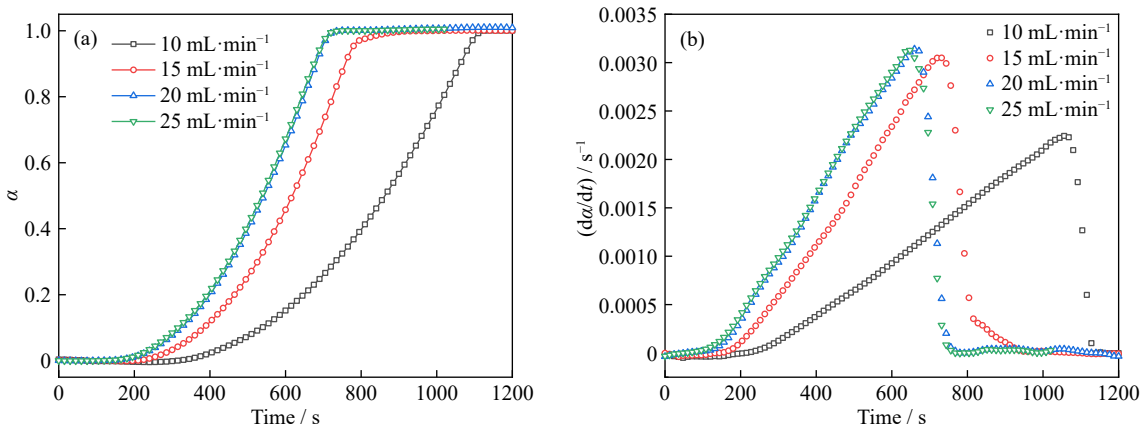

Fig. 4. (a) Reduction conversion curves and (b) conversion rate curves with time at different gas flow rates.

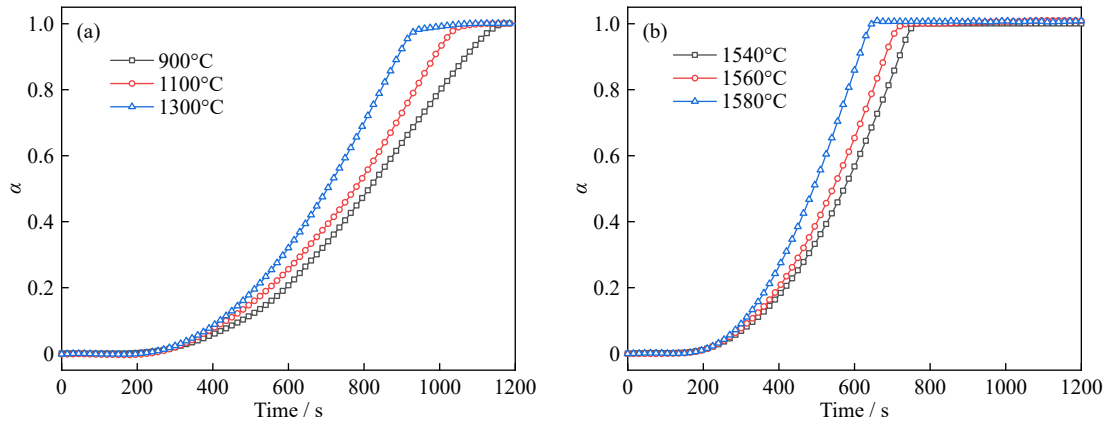

Fig. 5. Reduction conversion curves at different temperatures: (a) solid wustite and metal iron at 900–1300°C; (b) molten wustite and metal iron at 1540–1580°C.

the reduction conversion tends to increase with increasing reduction temperature for the same reduction time, regardless of the phase state of the reactants and products.

Fig. 6 shows the reduction conversion rate curves for the reduction of solid/molten wustite by hydrogen at different temperatures. The reduction rate curves are all single-peaked, independent of temperature and the phase state of the reactants and products. When the temperatures are 900, 1100, and 1300°C, the peak values of the reduction conversion curve are 0.00160, 0.00202, and 0.00227 s^{-1}, and the corresponding times are 927.0, 903.0, and 840.6 s, respectively. For the molten state, when the temperatures are 1540, 1560, and 1580°C, the peak values of the reduction conversion curve are 0.00305, 0.00315, and 0.00347 s^{-1}, and the corresponding times are 707.4, 661.2, and 591.0 s, respectively. Besides, as the reduction temperature increases, the peak of the reduction rate curve gradually moves to the left and becomes narrower, the peak value increases simultaneously, which indicates that the reduction reaction can reach a more intense state earlier.

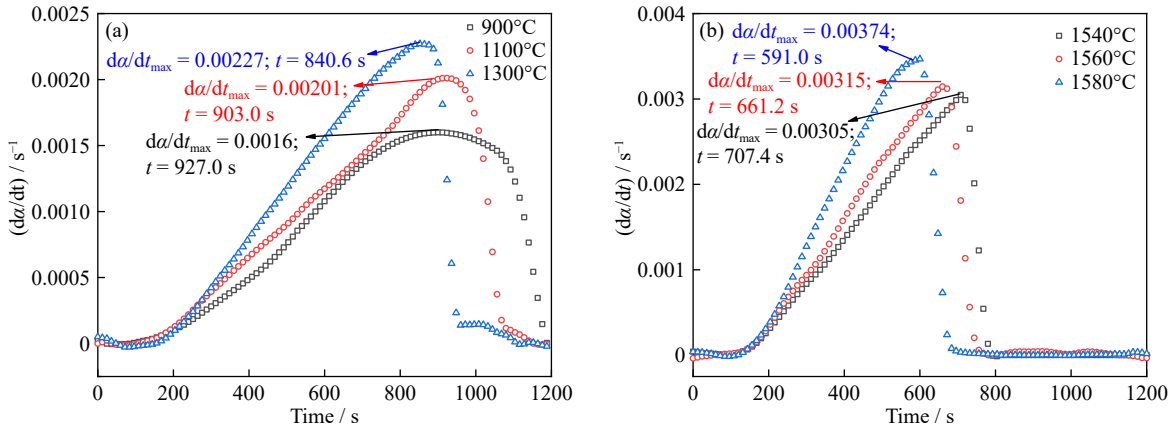

Fig. 6. Reduction conversion rate curves with time at different temperatures: (a) solid wustite and metal iron at 900–1300°C; (b) molten wustite and metal iron at 1540–1580°C.

3.3. Kinetic analysis

3.3.1. Model fitting method

A macro-kinetics model was established in the present work to further analyze the reduction mechanism of solid/liquid wustite by hydrogen. The reduction conversion of wustite during isothermal reduction by hydrogen is the function of reduction temperature and time, which can be expressed as:

$$\frac{d\alpha}{dt} = k(T) f(\alpha) \tag{2}$$

where $d\alpha/dt$ is reduction conversion rate; $k(T)$ is the reduction rate constant, which is the function of reduction temperature T; $f(\alpha)$ is the differential form of the reduction mechanism function; t is reduction time, s.

Previous studies [26–27] have shown that the integral method is suitable for the processing of isothermal thermal analysis kinetic data. Eq. (3) can be derived from Eq. (2):

$$G(\alpha) = \int_0^{\alpha} \frac{d\alpha}{f(\alpha)} = \int_0^{t} k(T)\,dt = k(T)t \tag{3}$$

where $G(\alpha) = \int_0^{\alpha} \frac{d\alpha}{f(\alpha)}$ is the integral form of the mechanism function.

It can be seen from Eq. (3) that $G(\alpha)$ is linearly related to the reduction time and the slope is the reduction rate constant $k(T)$ of the reaction at the corresponding temperature. $f(\alpha)$ is the most suitable mechanism function for the reduction process. The mechanistic functions commonly used for chemical reactions are shown in Table 2.

$k(T)$ can be determined by the Arrhenius equation:

$$k(T) = A\exp\left(-\frac{E}{RT}\right) \tag{4}$$

where A is the pre-exponential factor, s^{-1}; E is the activation energy, $kJ\cdot mol^{-1}$; R is the standard molar gas constant, $kJ\cdot mol^{-1}\cdot K^{-1}$.

Eq. (4) can be further expressed as:

$$\ln k(T) = -\frac{E}{RT} + \ln A \tag{5}$$

Eq. (5) shows that $1/T$ and $\ln k(T)$ are linearly related; the slope and intercept can determine the pre-exponential factor A and the activation energy E.

The experiment mainly uses the data when the conversion ratio is larger than 0.05 when determining the mechanism function to avoid the influence of the gas composition converting in the early reaction stage on the reduction process. In addition, record the time when the conversion was 0.05 as 0 s and when the conversion was greater than 0.05 as t'. The reduction rate constants $k(T)$ were calculated by linear fitting based on different $G(\alpha)$ in Table 2 and reaction time; the corresponding correlation coefficients are shown in Table 3. It can be found that the fitting effect of P_2 (Mampel Power, n = 1/2) is the best; the correlation coefficients (R^2) are all greater than 0.995. Therefore, $f(\alpha) = 2\alpha^{1/2}$ is the suitable mechanism function for the reduction of solid/liquid wustite by hydrogen. Fig. 7 shows the linear fitting results of $G(\alpha)$ vs. reaction time t' of the P_2 model, from which the reduction rate constant $k(T)$ can be calculated. Activation energy E and the pre-exponential factor A can be further determined by linear

Table 2. The mechanistic function models commonly used for chemical reactions

Code	Function	Differential form, $f(\alpha)$	Integral form, $G(\alpha)$
A_2	Avrami Erofeev Equation (n = 1/2, m = 2)	$2(1-\alpha)[-\ln(1-\alpha)]^{1/2}$	$[-\ln(1-\alpha)]^{1/2}$
A_3	Avrami Erofeev Equation (n = 1/3, m = 3)	$3(1-\alpha)[-\ln(1-\alpha)]^{2/3}$	$[-\ln(1-\alpha)]^{1/3}$
A_4	Avrami Erofeev Equation (n = 1/4, m = 4)	$4(1-\alpha)[-\ln(1-\alpha)]^{3/4}$	$[-\ln(1-\alpha)]^{1/4}$
P_2	Mampel Power (n = 1/2)	$2\alpha^{1/2}$	$\alpha^{1/2}$
P_3	Mampel Power (n = 1/3)	$3\alpha^{2/3}$	$\alpha^{1/3}$
P_4	Mampel Power (n = 1/4)	$4\alpha^{3/4}$	$\alpha^{1/4}$
D_2	Valensi Equation	$[-\ln(1-\alpha)]^{-1}$	$\alpha+(1-\alpha)\ln(1-\alpha)$
D_3	Jander Equation (2D, n = 2)	$(1-\alpha)^{1/2}[1-(1-\alpha)^{1/2}]^{-1}$	$[1-(1-\alpha)^{1/2}]^2$
D_4	Anti-Jander Equation	$3/2(1+\alpha)^{2/3}[(1+\alpha)^{1/3}-1]^{-1}$	$[(1+\alpha)^{1/3}-1]^2$
D_5	Zhuralev-Lesokin-Tempelman Equation (3D)	$3/2(1-\alpha)^{4/3}[(1-\alpha)^{-1/3}-1]^{-1}$	$[(1-\alpha)^{-1/3}-1]^2$
R_2	Cylinder Contraction (2D)	$2(1-\alpha)^{1/2}$	$1-(1-\alpha)^{1/2}$
R_3	Spherical Contraction (n = 1/3)	$3(1-\alpha)^{2/3}$	$1-(1-\alpha)^{1/3}$
R_4	Order of Reaction	$4(1-\alpha)^{3/4}$	$1-(1-\alpha)^{1/4}$
F_1	Mample Single Law (n = 1, m = 1)	$1-\alpha$	$-\ln(1-\alpha)$
F_2	Order of Reaction (n = 2)	$(1-\alpha)^2$	$(1-\alpha)^{-1}-1$
F_3	Order of Reaction	$1/2(1-\alpha)^3$	$(1-\alpha)^{-2}$

Note: n, m—Power exponents of empirical mechanism function; 2D—Two dimensional; 3D—Three dimensional.

Table 3. Correlation coefficients calculated using common reaction mechanism functions

Code	Temperature / °C					
	900	1100	1300	1540	1560	1580
A_2	0.9651	0.9465	0.9522	0.9453	0.9472	0.9529
A_3	0.9885	0.9770	0.9807	0.9764	0.9777	0.9811
A_4	0.9953	0.9872	0.9897	0.9869	0.9878	0.9900
P_2	0.9973	0.9999	0.9998	0.9999	0.9999	0.9998
P_3	0.9904	0.9963	0.9950	0.9975	0.9970	0.9950
P_4	0.9845	0.9918	0.9899	0.9936	0.9928	0.9898
D_2	0.8206	0.7774	0.7869	0.7678	0.7735	0.7878
D_3	0.7646	0.7167	0.7267	0.7062	0.7120	0.7276
D_4	0.9200	0.8931	0.8996	0.8853	0.8898	0.9000
D_5	0.4478	0.4003	0.4038	0.3784	0.3857	0.4017
R_2	0.9409	0.9172	0.9238	0.9131	0.9162	0.9244
R_3	0.9152	0.8865	0.8942	0.8823	0.8857	0.8950
R_4	0.8998	0.8688	0.8771	0.8645	0.8680	0.8780
F_1	0.8439	0.8061	0.8158	0.8014	0.8051	0.8169
F_2	0.5230	0.4761	0.4823	0.4597	0.4654	0.4806
F_3	0.2734	0.2403	0.2378	0.2141	0.2220	0.2315

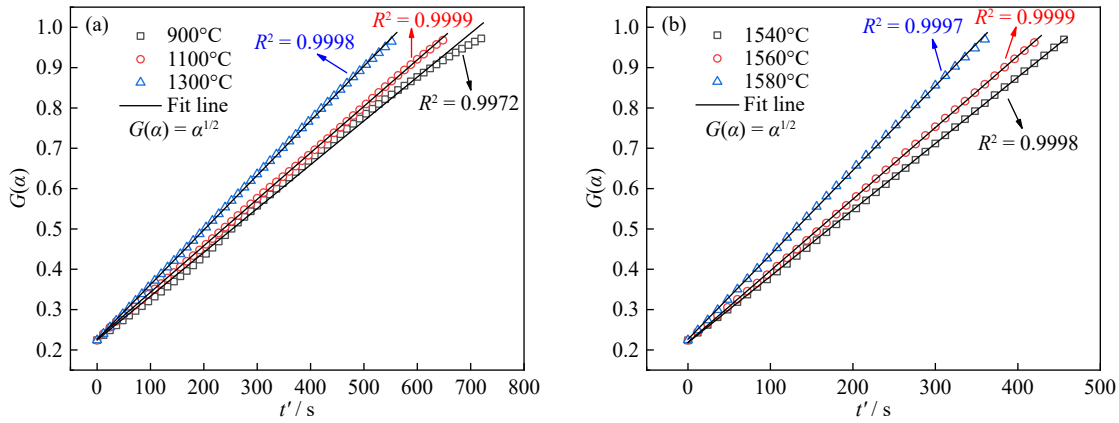

Fig. 7. Linear fitting of $G(\alpha)$ versus time of the reaction model (P_2): (a) 900–1300°C; (b) 1540–1580°C.

fitting of ln $k(T)$ vs. $1/T$ according to Eq. (5), and results are shown in Fig. 8.

The kinetic parameters fitted by P_2 (Mampel Power, n = 1/2) are shown in Table 4. It can be seen that the activation energy E is 6.99 kJ·mol^{-1} and the pre-exponential factor A is 0.00223 s^{-1} when both the reactants (wustite) and products (iron) are in the solid state. In comparison, the activation energy E is 115.75 kJ·mol^{-1}, and the pre-exponential factor A is 3.6136 s^{-1}, when both are in the molten state. The two values are significantly higher than those of the former state, especially the pre-exponential factor, which increases by nearly three orders of magnitude, indicating a higher reduction rate when the reactants and products are in the molten state. This may be due to the higher temperature causing a more intense movement of hydrogen molecules, which increases the frequency of contact between hydrogen molecules and FeO and ultimately makes the reaction rate increase. Kinetic equations for the reduction of wustite by hydrogen can be obtained by substituting E, A, and $f(\alpha) = 2\alpha^{1/2}$ into Eq. (2) and Eq. (4):

$$\frac{d\alpha}{dt} = 0.00223\exp\left(-\frac{6990}{8.314T}\right)\cdot 2\alpha^{1/2}$$

(FeO-solid; Fe-solid) (6)

$$\frac{d\alpha}{dt} = 3.6136\exp\left(-\frac{115750}{8.314T}\right)\cdot 2\alpha^{1/2}$$

(FeO-liquid; Fe-liquid) (7)

3.3.2. Iso-conversional method

The iso-conversional method is another method that has often been used to calculate the activation energy in thermal analysis kinetics. Eq. (8) can be obtained from Eq. (2) and Eq. (4):

$$\frac{d\alpha}{dt} = A\exp\left(-\frac{E}{RT}\right)f(\alpha) \quad (8)$$

Eq. (9) can be obtained by integrating Eq. (8):

$$\int_0^\alpha \frac{d\alpha}{f(\alpha)} = G(\alpha) = \int_0^t A\exp\left(-\frac{E}{RT}\right)dt = A\exp\left(-\frac{E}{RT}\right)t \quad (9)$$

Eq. (9) can be further expressed as:

$$\ln t = \ln G(\alpha) - \ln A + \frac{E}{RT} \quad (10)$$

When the reduction conversions α is a constant, then $\ln G(\alpha) - \ln A$ is also constant, so the slop of the plot $\ln t$ vs. $1/T$ can be used to calculate activation energy E. Therefore, the iso-conversional method has advantages that it can calculate the activation energy without determining the mechanism, and it can reflect the change of the activation energy at different reduction conversions [28–29].

Since the inert gas N_2 was used in the heating stage during the thermogravimetric test, the composition of the reducing

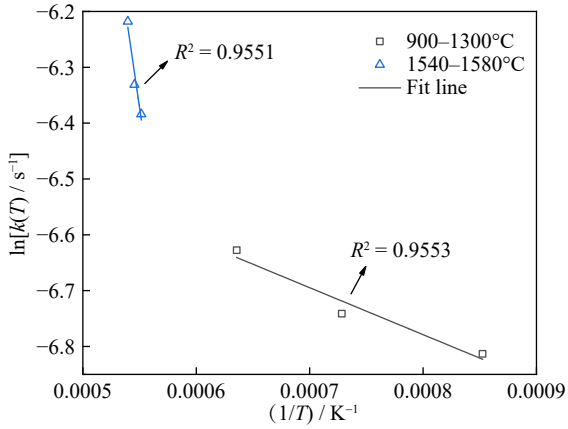

Fig. 8. Linear fitting results of $1/T$ and $\ln k(T)$.

Table 4. Kinetic parameters fitted by different mechanism function

Temperature / °C	$f(\alpha)$	R^2	$k(T)$ / s^{-1}	E / (kJ·mol^{-1})	A / s^{-1}
900		0.9973	0.00118		
1100	P_2: $f(\alpha) = 2\alpha^{1/2}$	0.9999	0.00132	6.99	0.00223
1300		0.9998	0.00169		
1540		0.9999	0.00136		
1560	P_2: $f(\alpha) = 2\alpha^{1/2}$	0.9999	0.00118	115.75	3.6136
1580		0.9998	0.00132		

gas could not reach the required gas composition immediately at the beginning of the reduction experiment, which resulted in a difference of the experimental conditions in early stage and later stage of reduction. Therefore, to ensure the reliability and rationality of the results, activation energy E of the reaction is calculated with the selected reduction conversion range of 0.2 to 0.9 with the step set to 0.1. The reaction time to reach each conversion ratio at different temperatures from Fig. 5 is used to further calculate the corresponding $\ln t$. Fig. 9 shows the linear relation between $\ln t$ and $1/T$, where the colored hollow symbols are calculated from experimental data, and the straight lines are obtained from linear fitting.

Activation energy E at different reduction conversions and the average activation energy during the entire reduction process are shown in Table 5. The correlation coefficients R^2 for activation energy calculation at all reduction conversions are greater than 0.95, which indicates the good correlation and high credibility of the results. The average activation energy is 5.85 kJ·mol^{-1} when the reactants and products are both in solid state and 104.74 kJ·mol^{-1} when they are both in molten state. The average activation energy calculated by the isoconversional method is in general agreement with the activation energy calculated by the Mampel Power model, indicating that the mechanism function selected by the model fitting method is accurate.

Fig. 10 shows the relationship between the activation energy and the reduction conversion when the reactants and products are in different phase states. When both reactants and products are in the solid phases, the activation energy increases with the increasing reduction conversion and ranges from 5.27 to 6.98 kJ·mol^{-1}. When the reactants and products are in the liquid phases, the range of activation energy at different reduction conversions is 84.44–112.84 kJ·mol^{-1}, and also shows an increasing trend; however, when the reduction conversion is greater than 0.3, the activation energy varies very little with the reduction conversion, which means the reduction rate is single step controlled. The results show that the activation energy of solid FeO and liquid FeO reduced by

Table 5. Activation energies at different α in different temperature ranges

α	Activation energy / (kJ·mol^{-1})		R^2	
	900–1300°C	1540–1580°C	900–1300°C	1540–1580°C
0.20	5.53	84.44	0.9970	0.9655
0.30	5.27	96.59	0.9741	0.9686
0.40	5.41	103.21	0.9561	0.9710
0.50	5.46	106.82	0.9506	0.9678
0.60	5.68	109.84	0.9522	0.9653
0.70	6.04	112.08	0.9547	0.9631
0.80	6.46	112.84	0.9646	0.9633
0.90	6.98	112.12	0.9771	0.9636
Average	5.85	104.74	—	—

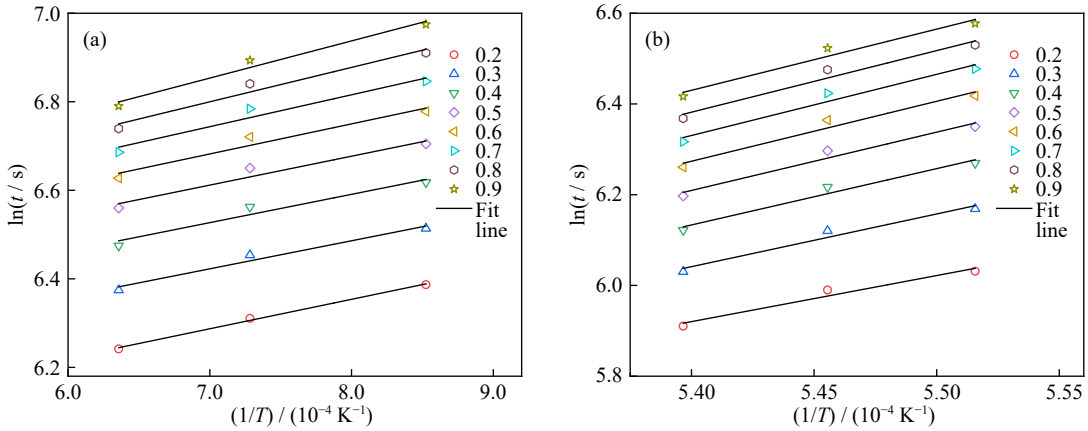

Fig. 9. Linear relation between $\ln t$ and $1/T$ with the reduction conversion range of 0.2–0.9: (a) 900–1300°C; (b) 1540–1580°C.

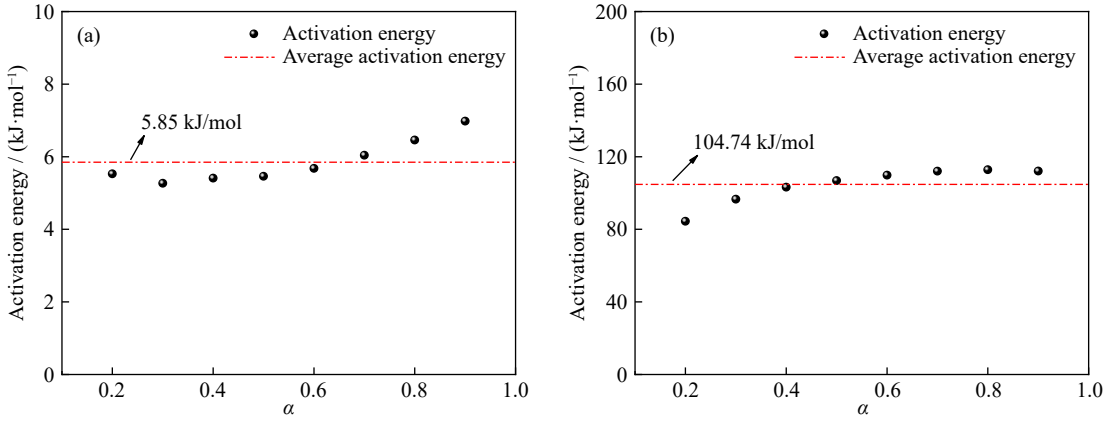

Fig. 10. Relationship between activation energy and reduction conversion: (a) 900–1300°C; (b) 1540–1580°C.

hydrogen are different, and the activation energy of solid FeO reduced by hydrogen is lower, which might be caused by the difference in the contact area between hydrogen and reactants [30].

4. Conclusions

The reduction process of solid/molten wustite by hydrogen and its reduction kinetics were investigated by isothermal thermogravimetric analysis, and the following conclusions were obtained.

(1) The complete reduction can be achieved regardless of the reduction temperature and phase states, while the reduction conversion increases with temperature at the same reduction time; the reaction processes are faster when both reactants and products are in molten state. The peak of the reduction rate curve moves to the left and becomes narrower when the temperature increases, meanwhile the peak value increases, indicating that the reduction reaction can reach a more intense state earlier.

(2) According to the results of the model fitting method, $f(\alpha) = 2\alpha^{1/2}$ is a suitable mechanism function for the reduction of wustite by hydrogen in different phase states. E is 6.99 kJ·mol^{-1} and A is 0.00223 s^{-1} when the reactants and products are in solid state; when both of them are in the molten state, E is 115.75 kJ·mol^{-1} and A is 3.6136 s^{-1}. More energy is required for the reduction of the molten phase, and meanwhile, the pre-exponential factor increases by nearly three orders of magnitude. Kinetic equations can be expressed as:

$$\frac{d\alpha}{dt} = 0.00223\exp(-\frac{6990}{8.314T})\cdot 2\alpha^{1/2} \text{ (FeO-solid; Fe-solid),}$$

$$\frac{d\alpha}{dt} = 3.6136\exp(-\frac{115750}{8.314T})\cdot 2\alpha^{1/2} \text{ (FeO-liquid; Fe-liquid).}$$

(3) According to the iso-conversional method, the calculated E values are 5.27–6.98 kJ·mol^{-1} at different reduction conversions with an average activation energy is 5.85 kJ·mol^{-1} when the reactants and products are in the solid state; when they are both in the molten state, E ranges from 84.44 to 112.84 kJ·mol^{-1}, and the average activation energy is 104.74 kJ·mol^{-1}. These values generally agree with those calculated by the Mampel Power model, so the mechanism function selected by the model fitting method is accurate.

Acknowledgements

This work was financially supported by the National Natural Science Foundation of China (Nos. 51874025 and 52174291).

Conflict of Interest

All authors have no financial/commercial conflicts of interest.

References

[1] X.Y. Wang, B. Li, C. Lü, *et al*., China's iron and steel industry carbon emissions peak pathways, *Res. Environ. Sci.*, 35(2022), No. 2, p. 339.

[2] Y.J. Shao, L. Xu, X.P. Liu, and H.Z. Chen, Discussion on solution of "carbon neutrality" in China's steel production, *China Metall.*, 32(2022), No. 4, p. 1.

[3] Y. Xin, Y.K. Cui, J.L. Tian, *et al*., Application status and prospect of low carbon technology in iron and steel industry, *Chin. J. Eng.*, 44(2022), No. 4, p. 801.

[4] R. Liu, Z.F. Zhang, X.J. Liu, X. Li, H.Y. Li, and Q. Lü, Development trend and prospect of low-carbon green ironmaking technology, *Iron Steel*, 57(2022), No. 5, p. 1.

[5] V. Vogl, M. Åhman, and L.J. Nilsson, Assessment of hydrogen direct reduction for fossil-free steelmaking, *J. Cleaner Prod.*, 203(2018), p. 736.

[6] T. Ariyama, Perspective toward long-term global goal for carbon dioxide mitigation in steel industry, *Tetsu-to-Hagane*, 105(2019), No. 6, p. 567.

[7] F. Li, M.S. Chu, J. Tang, *et al*., Thermodynamic performance analysis and environmental impact assessment of an integrated system for hydrogen generation and steelmaking, *Energy*, 241(2022), art. No. 122922.

[8] J. Tang, M.S. Chu, F. Li, C. Feng, Z.G. Liu, and Y.S. Zhou, Development and progress on hydrogen metallurgy, *Int. J. Miner. Metall. Mater.*, 27(2020), No. 6, p. 713.

[9] D. Spreitzer and J. Schenk, Reduction of iron oxides with hydrogen—A review, *Steel Res. Int.*, 90(2019), No. 10, art. No. 1900108.

[10] M.N.A. Tahari, F. Salleh, T.S.T. Saharuddin, A. Samsuri, S. Samidin, and M.A. Yarmo, Influence of hydrogen and carbon monoxide on reduction behavior of iron oxide at high temperature: Effect on reduction gas concentrations, *Int. J. Hydrogen Energy*, 46(2021), No. 48, p. 24791.

[11] Z.Y. Chen, J. Dang, X.J. Hu, and H.Y. Yan, Reduction kinetics of hematite powder in hydrogen atmosphere at moderate temperatures, *Metals*, 8(2018), No. 10, art. No. 751.

[12] C.Y. Ding, X.W. Lv, G. Li, *et al*., Isothermal reduction of powdery $2CaO{\cdot}Fe_2O_3$ and $CaO{\cdot}Fe_2O_3$ under H_2 atmosphere, *Int. J. Hydrogen Energy*, 43(2018), No. 1, p. 24.

[13] H.B. Zuo, C. Wang, J.J. Dong, K.X. Jiao, and R.S. Xu, Reduction kinetics of iron oxide pellets with H_2 and CO mixtures, *Int. J. Miner. Metall. Mater.*, 22(2015), No. 7, p. 688.

[14] J. Tang, M.S. Chu, F. Li, Y.T. Tang, Z.G. Liu, and X.X. Xue, Reduction mechanism of high-chromium vanadium–titanium magnetite pellets by H_2–CO–CO_2 gas mixtures, *Int. J. Miner. Metall. Mater.*, 22(2015), No. 6, p. 562.

[15] J.L. Zhang, G.Q. Zhang, Z.J. Liu, Z.H. Wang, K.J. Li, and X.B. Zhang, Production overview and main characteristics of HIsmelt process in Shandong Molong, *China Metall.*, 28(2018), No. 5, p. 37.

[16] R. Sripriya, T. Peeters, K. Meijer, C. Zeilstra, and D. van der Plas, Computational fluid dynamics and combustion modelling of HIsarna incinerator, *Ironmaking Steelmaking*, 43(2016), No. 3, p. 192.

[17] L.Y. Xing, Z.S. Zou, Y.X. Qu, L. Shao, and J.Q. Zou, Gas-solid reduction behavior of in-flight fine hematite ore particles by hydrogen, *Steel Res. Int.*, 90(2019), No. 1, art. No. 1800311.

[18] H. Katayama, S. Taguchi, and N. Tsuchiya, Reduction of iron oxide in molten slag with H_2 gas, *Tetsu-to-Hagane*, 68(1982), No. 15, p. 2279.

[19] S. Ban-Ya, Y. Iguchi, and T. Nagasaka, Rate of reduction of liquid wustite with hydrogen, *Tetsu-to-Hagane*, 70(1984), No. 14, p. 1689.

[20] S. Hayashi and Y. Iguchi, Hydrogen reduction of liquid iron oxide fines in gas-conveyed systems, *ISIJ Int.*, 34(1994), No. 7, p. 555.

[21] T. Nagasaka, M. Hino, and S. Ban-Ya, Interfacial kinetics of hydrogen with liquid slag containing iron oxide, *Metall. Mater.*

Trans. B, 31(2000), No. 5, p. 945.
[22] M.N. Seftejani and J. Schenk, Kinetics of molten iron oxides reduction using hydrogen, [in] *7th International Congress on Science and Technology of Steelmaking*, Venice, 2018.
[23] B.L. Hou, H.Y. Zhang, H.Z. Li, and Q.S. Zhu, Study on kinetics of iron oxide reduction by hydrogen, *Chin. J. Chem. Eng.*, 20(2012), No. 1, p. 10.
[24] W.K. Jozwiak, E. Kaczmarek, T.P. Maniecki, W. Ignaczak, and W. Maniukiewicz, Reduction behavior of iron oxides in hydrogen and carbon monoxide atmospheres, *Appl. Catal. A*, 326(2007), No. 1, p. 17.
[25] Y. Zhou, Y.M. Gao, X.J. Ma, X. Zheng, M. Wang, and B. Wang, Preparation of FeO and its stability at room temperature, *J. Wuhan Univ. Sci. Technol.*, 36(2013), No. 5, p. 383.
[26] Y.S. Sun, Y.X. Han, P. Gao, and G.F. Li, Investigation of kinetics of coal based reduction of oolitic iron ore, *Ironmaking Steelmaking*, 41(2014), No. 10, p. 763.
[27] S. Vyazovkin, A.K. Burnham, J.M. Criado, L.A. Pérez-Maqueda, C. Popescu, and N. Sbirrazzuoli, ICTAC Kinetics Committee recommendations for performing kinetic computations on thermal analysis data, *Thermochim. Acta*, 520(2011), No. 1-2, p. 1.
[28] R.S. Xu, J.L. Zhang, G.W. Wang, *et al*., Isothermal kinetic analysis on fast pyrolysis of lump coal used in COREX process, *J. Therm. Anal. Calorim.*, 123(2016), No. 1, p. 773.
[29] S. Ren and J.L. Zhang, Thermogravimetric analysis of anthracite and waste plastics by iso-conversional method, *Thermochim. Acta*, 561(2013), p. 36.
[30] C.Y. Ding, X.W. Lv, S.W. Xuan, K. Tang, and C.G. Bai, Isothermal reduction kinetics of powdered hematite and calcium ferrite with CO–N_2 gas mixtures, *ISIJ Int.*, 56(2016), No. 12, p. 2118.